Main Manuscript for

Xenosiderophore transporter gene expression and clade-specific filamentation in *Candida auris* killifish infection

Hugh Gifford[a], Tina Bedekovic[a], Nicolas Helmstetter[a], Jack Gregory[a], Qinxi Ma[a], Alexandra C. Brand[a], Duncan Wilson[a], Johanna Rhodes[b,c], Mark Ramsdale[a], Tetsuhiro Kudoh[d,1], Rhys A. Farrer*[a,1]

[a]MRC Center for Medical Mycology, University of Exeter, Geoffrey Pope Building, Stocker Road, Exeter, United Kingdom, EX4 4QD

[b]Department of Medical Microbiology, Radboudumc, Geert Grooteplein Zuid 10, Nijmegen, Netherlands, 6525 GA

[c]MRC Centre for Global Infectious Disease Analysis, Imperial College London South Kensington Campus, London, United Kingdom, SW7 2AZ

[d]Biosciences, University of Exeter, Geoffrey Pope Building, Stocker Road, Exeter, United Kingdom, EX4 4QD

[1]Co-Senior Author

Corresponding Author: Rhys Farrer

Email: R.Farrer@exeter.ac.uk

Author contributions: Designed research: All authors. Performed research: HG, TB, NH, JG, QM. Analysed data: HG. Wrote the paper: All authors.

Competing interest statement: No competing interests.

Classification: Biological sciences, Microbiology.

Pre-print: This article has been previously made available as a pre-print *via* the bioRxiv server.

Keywords: *Candida auris*, *Aphanius dispar*, dual host-pathogen RNA-seq, siderophore transport, filamentation

This PDF file includes:

Main text

Figures 1-4

Abstract

Candida auris is a World Health Organization (WHO) critical priority fungal pathogen. An associated mortality of ~45%, rising drug resistance and massive nosocomial outbreaks complicate clinical treatment. A critical bottleneck in understanding virulence is the lack of gene expression profiling models during *in vivo* host tissue infection. We developed a thermo-relevant fish embryo yolk-sac (*Aphanius dispar*; Arabian killifish; AK) microinjection model at human body temperature featuring clinically relevant features of host immunity. This allowed us to interrogate infection dynamics through dual host-pathogen RNA-seq at 24 and 48 h post injection (HPI) at 37 °C across five major clades (I-V) of *C. auris*. Host responses to infection featured heat shock, complement activation, and nutritional immunity, including haem oxygenase (*HMOX*) expression in response to clade IV infection. We identified an *in vivo* transcriptional signature across five clades of *C. auris* that was highly enriched for putative xenosiderophore transmembrane transporters. We describe this newly-discovered seventeen-member xenosiderophore transporter candidate (*XTC*) family in terms of individual gene expression patterns, and a sub-clade of five putative haem transport-related (*HTR*) genes. Only the basal clade V isolate formed filaments during infection, coinciding with typical and atypical regulators of morphogenesis, including *UME6*, *HGC1*, and the novel adhesin *SCF1*. Clades I and IV demonstrated increased virulence, coinciding with up-regulation of three *HTR* genes in clade IV, and the mating-type locus (*MTL*) non-mating gene *PIKA* in both. Our study provides critical insights into the pathogenesis of C. auris, including species-wide up-regulation of *XTC* and *HTR* genes during clinically relevant *in vivo* host tissue infection.

Significance statement

Candida auris is an emerging human fungal pathogen and global public health threat, but *in vivo* tissue infection transcriptome analysis has not been achieved with available models. We infected Arabian killifish yolk-sacs to study gene expression programmes by five clades of *C. auris*. We discovered that the basal clade V uniquely filamented during infection. Additionally, all clades encode a large expanded family of xenosiderophore transporters that are upregulated during infection. These results highlight the important roles for morphology switching and iron acquisition during infection, both of which shed light on its mechanisms of infection and could make novel drug targets.

Main text

Introduction

C. auris is an ascomycetous yeast that has rapidly transitioned from recent emergence to global public health threat (1) and World Health Organization (WHO) critical priority human fungal pathogen (2). The oldest known historical isolate is from 1996 (3) and it was first recognised as a species in 2008 (4). Over the last decade, *C. auris* had caused nosocomial outbreaks globally resulting in intensive care unit (ICU) shutdowns and massive infection control costs (5–7). Worryingly, *C. auris* is now a leading cause of invasive candidiasis in several hospital settings globally (8, 9). Distinct clades of *C. auris*, including a recent sixth clade (10, 11), suggest that multiple populations of *C. auris* have simultaneously emerged from an unknown niche, all of which are highly adapted for human infection (12, 13). Clade-specific differences have been noted, including clades I, III, and IV more commonly associated with invasive disease and nosocomial outbreaks, while clades II and V have been primarily reported in cases of otomycosis and rarely in bloodstream infection (14). Human mortality associated with *C. auris* candidaemia is potentially higher with clades I and IV than clade III, but this difference has not been shown to be statistically significant (15). Clade and strain-specific genotypic and phenotypic variation may underlie differences in clinical presentation and pathogenesis.

C. auris bloodstream infection is associated with a human mortality of ~45% (16). Owing to the recency of its emergence, the factors governing in-host fitness and virulence during infection are poorly understood. *C. auris* has been shown to reproduce as budding yeasts in mammalian tissues (17, 18) and possess multiple adhesins associated with an aggregation phenotype (19, 20). There has been no evidence of toxin synthesis unlike distantly related *C. albicans* (21, 22). *C. auris* digests of host tissue through secreted aspartyl proteases (23) and evades host immune responses through cell surface masking (24) and intra-phagocytic survival with cell lysis (25). *C. auris* also demonstrates high rates of azole antifungal drug resistance and a rising incidence of pan-drug resistance (26).

Gene expression profiling has become a standard approach for assessing host and pathogen responses to infection. However, no experiment has described the gene expression of *C. auris* during *in vivo* infection of living tissue to date. Studies assessing the transcriptome in an *in vivo* murine catheter model (27), human whole blood *ex vivo* (28), co-incubation with human dermal fibroblasts (29) or murine cell line-derived macrophages (30) have been informative. Additionally, host responses have been assessed in murine peripheral skin (31), human peripheral blood-derived monocytes (32), and murine bone marrow-derived macrophages (33). However, these studies have not reported adequate pathogen RNA recovery to interrogate in-host pathogen expression, except for the dual RNA-seq study using the

102 *ex vivo* whole blood model, for which it was possible to compare gene expression profiles between
103 *C. auris* and other *Candida* species (28).
104
105 The dearth of studies profiling host-pathogen gene expression *in vivo* for *C. auris* infection may
106 relate to the lack of a model which allows adequate RNA recovery, balanced with a reasonable degree of
107 clinical relevance. Most murine models, such as BALB/c (17, 34–36) and C57BL/6 mice (33), have only
108 very rarely demonstrated lethality through *C. auris* infection (32, 37, 38) without major
109 immunosuppression with cyclophosphamide/cortisone (39–50), monoclonal antibody neutrophil depletion
110 (18, 51), or other immunodeficiency (19, 52, 53). Additionally, mouse models are also expensive and
111 associated with concerns over environmental pathogen shedding (54). Alternative host models such as
112 *Galleria mellonella* (34, 44, 55–61), *Drosophila melanogaster* (62) and *Caenorhabditis elegans* (60) have
113 been employed, but these may lack key elements of mammalian-relevant immune systems, thus limiting
114 their scope of application. In patients, immune control of *C. auris* is thought to depend on myeloid cell
115 activity *via* C-type lectin receptors such as complement receptor 3 and mannose receptor MMR, followed
116 by interleukin (IL)-17 pathway activation (63, 64). Therefore, an animal model that aligns with these
117 mechanisms will assist human-relevant profiling of host-pathogen interactions.
118
119 Fish larvae must survive hostile and varied ocean environments, demonstrating very early innate
120 immune responses such as antimicrobial peptide production and the complement cascade (65, 66). Only
121 in adulthood are teleost fish expected to possess functional IL-17 subtypes (A and F) that lead to T-
122 helper-17 subset differentiation and adaptive immunity in response to fungal infection (67). The zebrafish
123 (*Danio rerio*) model has allowed hindbrain (24, 68) and swim bladder (69) microinjection modelling of
124 *C. auris* infection, but rarely at temperatures above 30 °C, which zebrafish are broadly intolerant of. There
125 have been no in-host transcription studies using the zebrafish model. Fungal transcriptional programmes
126 can vary greatly across temperatures and are critical for mammalian pathogenesis (70–72). A
127 thermotolerant teleost fish embryo model such as the *Aphanius dispar*, also known as the Arabian killifish
128 (AK), which can acclimatise to temperatures up to and including 40 °C (73–76), offers a balance between
129 considerations of suitability for experimental manipulation and applicability to human fungal infection at
130 mammalian temperatures.
131
132 The environmental origins of *C. auris* have not been conclusively demonstrated. However, a
133 marine origin has been hypothesised and supported by successful isolation of *C. auris* in coastal waters
134 of both Indian and Pacific oceans (77, 78). Notably, a close relative of *C. auris* in the *Metschnikowiaceae*
135 clade, *C. haemulonii*, was first isolated in 1961 from the gut of blue-striped grunt (genera name
136 "*Haemulon*" for their blood-red mouth interior) (79). Therefore, a marine model could shed light on a
137 possible evolutionarily adaptive niche relevant not only to human infection but also to hypothetical origins

138 in an emerging pathogen. Additionally, fish embryo models align with the principles of replacement,
139 refinement and reduction of animals in laboratory research and offer a opportunity to develop novel
140 clinically relevant models with ethical benefits over models such as adult mice (80).
141
142 In this paper, we present the first study exploring in-host virulence of *C. auris* clades I-V in the AK
143 yolk-sac microinjection model at 37 °C. We supplemented our validation of the model with histology,
144 fungal burden recovery, and dual host-pathogen RNA-seq. By comparing *in vivo* and *in vitro* expression
145 profiles of *C. auris*, we detected a cross-clade expression signature that was significantly enriched for
146 siderophore transporter *SIT1* paralogues, which mediate uptake of siderophores produced by other
147 microbes (xenosiderophores). We designated this expanded gene family as xenosiderophore transporter
148 candidates (*XTC*), which included a haem transport-related (*HTR*) sub-clade. We also identified *in vivo*
149 filamentation by clade V during infection, which was associated with orthologues of key hypha-associated
150 genes from *C. albicans*. Together, these findings substantially enhance our knowledge of the processes
151 employed by *C. auris* during infection.
152
153 **Results**
154
155 Our AK yolk-sac microinjections with each of the five *C. auris* clades demonstrated lethality
156 (defined by cessation of heartbeat, **Figure 1A**) at 37 °C (92-100% *vs* 6% for sham injections). *C. auris*
157 was significantly more lethal at earlier timepoints for clade I (*vs* II, III or V) and clade IV (*vs* II or III), with
158 $p < 0.001$ and $p < 0.04$ respectively (**Figure 1B**, **Table S1**). We compared histological sectioning of
159 *C. auris* in the AK yolk-sac at 48 HPI to understand morphological consequences of *C. auris* infection. All
160 clades of *C. auris* grown *in vitro* and *in vivo* exhibited budding yeast morphologies, except for the clade V
161 strain, which demonstrated predominantly filamentous forms grown *in vivo* (**Figure 1C**). Only minor inter-
162 clade differences were recorded for growth rate and counts of colony-forming units (CFU). Specifically,
163 clade II was slower growing in YPD-broth at 37 °C (**Figure S1A**), a difference that was not later identified
164 in CFUs recovered from infected AK embryos (**Figure 1D**). A mean average ($\bar{x}$) of 673 CFUs were
165 recovered per infected embryo, which increased 166x 24 h post injection (HPI, $\bar{x}$ = 1.12 x10^5) and a
166 further ~60% after 48 HPI ($\bar{x}$ = 1.78 x10^5). Filamentous clade V colonies were then grown on YPD-agar,
167 demonstrating rough (as opposed to smooth) colonies in approximately 1-2% of plated colonies (**Figure**
168 **S1B**), which consisted of elongated yeast cells and filamentous structures (>10-50 μm) consistent with
169 pseudohyphae (**Figure S1C**). These results indicate that AK embryo yolk-sac microinjection is resulting in
170 an active *C. auris* infection, which is associated with death after 7 d, and therefore is an informative model
171 for the study of human fungal pathogens such as *C. auris*.
172

173 To characterize host responses to *C. auris* during infection, we identified host differentially
174 expressed genes (DEGs) between infection by each clade and sham injections. We identified 685 DEGs
175 during infection with any clade (2.49% potential genes), of which 183 were up-regulated and 508 were
176 down-regulated in response to at least one clade. There were no host DEGs common to infection by all
177 five clades. Only four up-regulated genes and one down-regulated gene was shared across host
178 responses to four clades of infection (**Table S2**). Up-regulated genes in 4/5 clades included Laminin
179 subunit alpha-1 (*LAMA1*), Glucose-6-phosphatase (*G6PC*), DN117939 (hypothetical protein) and
180 Tryptophan aminotransferase protein 1 (*TAR1*). The immunoglobulin-like fibronectin type III domain-
181 containing protein 1 (*IGFN1*) was down-regulated in 4/5 clades. These results suggest AK larvae have
182 only a subtle non-uniform response to each clade of *C. auris* microinjection at these time-points, also
183 potentially reflecting differences in virulence between strains and stages of infection.
184
185 While a common host response to all clades of *C. auris* was not identified, we did identify clade-
186 specific host responses to infection. At 24 HPI, clade II elicited the greatest host response, with 41 up-
187 regulated genes and 210 down-regulated genes (**Figure 2A**). Reassuringly, we detected very few
188 differences between sham injection and no injection (**Figure 2B**, SI Appendix). At 48 HPI, clade IV
189 elicited the greatest host response, with 49 up-regulated genes and 104 down-regulated genes).
190 Importantly, we found differential expression of heat shock proteins (*HSP30* and *HSP70*), complement
191 cascade elements, pattern recognition receptors (PRRs), inflammatory transcription regulators, and
192 modulators of nutritional immunity with higher log-fold changes in clades I and IV, especially at 48 HPI
193 (**Figure 2C**). The most prominent gene relevant to pathogen recognition was *CARD14* in clade I and IV
194 infection at 48 HPI (**Figure 2D-E**). We found *NLRP3* (inflammasome) expression during clade III infection
195 at 24 HPI. Several significantly enriched functional terms were identified from our DEGs, especially
196 among the more virulent clades I and IV at 48 HPI. Host transcriptional response to clade I infection
197 included 15 enriched GO terms, driven by up-regulation of two orthologues of *LAMA1* and *LAMA2*
198 (**Figure 2D**). Clade IV had significant changes in functional annotation related to haem catabolism, haem
199 binding, and haem oxygenase (*HMOX*). Two orthologues of *HMOX* drove most of these enrichments,
200 such as haem oxidation (log-fold change $\bar{x}$ = 3.96, FDR < 0.0003, **Figure 2E**, **Figure S2**). Another host
201 up-regulated gene from infection by clade IV was ferroxidase hephaestin (*HPHL1*), which is also involved
202 in iron nutritional immunity. Together, these findings suggest that heat shock proteins, nutritional immunity
203 (particularly iron acquisition), and the complement effect system are important elements of the AK larval
204 response to *C. auris*.
205
206 We compared the in-host transcriptome to expression induced by growth in a standard rich
207 laboratory media (YPD). Principle components and sample correlation clustering from gene expression
208 data indicated a predominant separate clustering of *in vivo vs in vitro* conditions, indicating that the gene

209 expression profile of *C. auris* during infection is substantially different to that when it is grown in nutrient-
210 rich laboratory media (**Figure S1G and S1H**). We identified 960 DEGs between *in vivo* AK infection at
211 24 HPI or 48 HPI *vs in vitro* culture in YPD over 24 h (499 up-regulated, 523 down-regulated, 17.7% of
212 potential genes, **Figure 3A**). We identified few DEGs between the two time-points 24 HPI to 48 HPI, with
213 zero DEGs for clade IV and V between those time points (**Figure S3A**). The highest numbers of up-
214 regulated DEGs were identified in the filamentous clade V at 24 HPI and in the more virulent clades I and
215 IV at 48 HPI (**Figure S3B-C**). Six functional annotation terms were enriched across all in-host infections
216 at 48 HPI, related to major superfacilitator family carbohydrate and siderophore-iron transmembrane
217 transport (**Figure S4**). Together, this analysis reveals that during infection, which is a nutrient-limited
218 environment, *C. auris* is responding by significantly increasing expression of genes involved in sugar
219 uptake, as well as members of the *C. auris* expanded gene family of siderophore transporters.
220
221 Thirteen DEGs common to all clades of in-host transcription were transmembrane transporters,
222 including up-regulation of transporters for xenosiderophores (*SIT1* genes 3921 and 1487), sugar
223 transporters (*HGT2*, *HGT12*), an ammonia transporter (*ATO2*), and a nicotinic acid transporter (*TNA1*).
224 We also found down-regulation of several drug-resistance-related efflux pumps (*MDR2* and *DTR1*) and
225 peptide transporters (*TPO3*, *PTR22*, **Figure 3B**, **Table S3**). Surprisingly, several putative virulence
226 factors such as lipase *LIP1* and cell wall-related *KRE6* and *SOD6* were also down-regulated across all
227 five clades, as were *ALS4* and *MDR1* in at least one clade (**Figure 3C**). Several members of the *SIT1*
228 family were differentially expressed by <5 of the clades including 0002, 1457, 1458, 1542,2110, 2241,
229 2465, 3908 and 4097. Meanwhile, two *SIT1* genes were down-regulated across 3 of the clades (1519 and
230 1499). Several *SIT1* genes were upregulated in ≥1 clade and down-regulated in ≥1 clade (3908 and
231 2465). The strong signal of differential expression in the *SIT1* expanded gene family highlights the
232 potential importance during in-host survival.
233
234 The more virulent clades (I and IV) are **a**-type mating type locus (*MTL*), while the less virulent
235 clades (II, III and V) contain the **α**-type *MTL*. Surprisingly, we found differential expression in several non-
236 mating genes between more virulent and less virulent clades, including poly-A polymerase (*PAP1*),
237 oxysterol binding protein (*OBPA*) and phosphatidylinositol 4-kinase (*PIKA*, **Figure S5B**). Within the set of
238 10 DEGs shared across all comparisons, several genes outside the *MTL* were up-regulated, including
239 vacuolar protein sorting gene, *VPS70*, and filamentous growth regulator, *FGR14*. Additionally, the drug
240 efflux pump, *MDR1*, was down-regulated across all comparisons, supporting the idea of a fitness trade-off
241 between resistance and virulence.
242
243 To explore drivers of filamentation by the clade V strain, we identified 1,046 DEGs between clade
244 V and each of the other clades (I-IV), comprising 601 up-regulated and 526 down-regulated genes across

245 all comparisons. We identified a set of 57 genes shared across all comparisons for *in vivo* conditions only,
246 since we did not observe filamentation in nutrient-rich YPD. Twenty-two genes were up-regulated at
247 24 HPI, seven at 48 HPI, and 18 at both time-points (**Figure S5C**). Most of the up-regulated genes were
248 metabolic (*n* = 13), including two cytochrome P450 *ERG5* orthologues, though *ERG11* was down-
249 regulated. Transmembrane transporters for sugar (including two *HGT13* orthologues), amino acids and
250 siderophores (*SIT1* 1487) were also up-regulated (*n* = 10). Cell wall genes up-regulated in filamentous
251 clade V (*n* = 8) included the novel adhesin *SCF1*, GPI-anchored genes *PGA31* and *IFF4*, and orthologues
252 of classical *C. albicans* hyphal adhesins *ALS3* and *RBR3*. We identified differentially expressed
253 transcription factors and related regulators, such as *HAP41* and the pheromone receptor *STE2*, which
254 could play a governing role on these responses.
255
256 We examined significant DEGs between clade V and at least one other clade using mean-log fold
257 change (**Figure S5D**). Several genes that play critical roles in *C. albicans* hypha formation were highly
258 up-regulated, such as transcription factor *UME6* and hypha-specific G1 cyclin-dependent protein
259 serine/threonine kinase *HGC1*. Enrichment analysis indicated up-regulated gene sets involving CFEM
260 domain, cytochrome P450/oxidoreductase activity, hypha-regulated cell wall GPI-anchored proteins and
261 siderophore transport, particularly at 24 HPI and comparing clade V to clade II (**Figure S5D**). Significantly
262 up-regulated iron-related transport genes in clade V included *FRE3*, *CFL4*, *FRP1*, and *SIT1* genes 1487,
263 1499, 1519, 1542, and 4097. This is consistent with the preservation of a major filamentation programme
264 in *C. auris*, demonstrated in the basal clade V.
265
266 Given the prominence of *SIT1* orthologues across the transcriptomic analyses of *C. auris* during
267 *in vivo* gene expression, we set out to characterise the structural and evolutionary conservation of the
268 expanded gene family across orthogroups, including outgroup species *C. haemulonii* and *C. albicans*. We
269 performed phylogenetic analysis on proteins with sequence similarity across seven orthologue clusters, of
270 which two main groupings of transporters with 14 transmembrane domains (TMRs) emerged (**Figure 4**).
271 The first group included genes with functional annotation relating to siderophore import (including 12
272 genes in clade I). The second group included haem transmembrane import genes (including 5 genes in
273 clade I). Most of the orthologues retained 14 TMRs, and few had evidence of additional annotations
274 except for the trichothecene mycotoxin efflux pump PFAM domain across multiple groupings. The
275 orthologue *SIT1* 1547 contained 12 TMRs and was up-regulated with *SIT1* 1548 containing 2 TMRs,
276 which was not identified as a *SIT1* orthologue in our pipeline but has previously been described as such
277 (28, 81).
278
279 To explore the evolutionary history of *SIT1*-related genes in fungi, we identified 1,689 homologs
280 of *C. albicans SIT1* across 304 reference genomes from 226 fungal species, which clustered into two

281 branches: a smaller branch annotated for siderophore transport including the 12 *C. auris* groupings which
282 we have designated "xenosiderophore transporter candidates" (*XTC*), and a larger branch featuring
283 genes predicted (by GO term) to encode haem transporters, including the 5 *C. auris* groupings, which we
284 have additionally designated "haem transport-related" (*HTR*, **Figure S6A**). There were no putative haem
285 transporters or members of the larger branch for *C. albicans*, which only contained the single *SIT1* gene.
286 The most prominent expansion of the *XTC* branch in the *Metschnikowiaceae* clade was in *C. haemulonii*
287 (*n* = 15), followed by *C. auris* (*n* = 12). *XTC* orthologues were not present in any members of the basal
288 *Blasocladiomycota*, *Chytridiomycota* and *Mucoromycota*, or in several *Ascomycota* (e.g. *Pichia*
289 *kudriavzevii*, *Schizosaccharomyces pombe* and *Pyricularia oryzae*) and Basidiomycota (e.g. *Ustilago*
290 *maydis*). Common human fungal pathogens such as *Aspergillus fumigatus*, *C. albicans* and
291 *Nakaseomyces glabratus* contained only one *XTC* orthologue (**Figure S6B**). The *HTR* clade, by contrast,
292 was more prominent across fungal phyla, with as many as nine in *Mucor* species, 16 in *A. flavus* and 22
293 in *F. solani*. We therefore propose a naming of these two expanded gene families as *XTC1-12* and *HTR1-*
294 *5* in *C. auris*.
295
296 *C. auris* demonstrates clade-specific *XTC* presence-absence polymorphisms including the
297 absence of *XTC5* in clade V, *XTC10* in clade IV, and *XTC4*, *XTC9* and *XTC11* in clade II (**Figure S6C**).
298 Clade II exhibited the greatest degree of *XTC* gene loss. Additionally, the AK embryo expressed *HMOX*
299 genes during clade IV infection, while clade IV up-regulated *HTR1*, *HTR2* and *HTR5*. This suggests a
300 specific host-pathogen interaction axis in nutritional immunity related to haem scavenging. No other
301 clades of infection were associated with such iron-related functional enrichment in the host, and no other
302 clades expressed more than one *HTR* gene. Overall, eleven *XTC* genes were differentially expressed in-
303 host compared to *in vitro* growth, including up-regulation of *XTC1*, *XTC2*, *XTC3*, *XTC4*, *XTC6*, *XTC7*,
304 *XTC11* and *XTC12*, and down-regulation of *XTC8*, *XTC9* and *XTC12* in at least one clade. In-host up-
305 regulation of *XTC3* and *XTC7* was significant across all clades. Additionally, the more virulent clades
306 were associated with up-regulation of *XTC4*, *XTC5*, and *XTC8*. The filamentous clade V up-regulated
307 *XTC7* across comparisons with all other clades, and up-regulated *XTC1*, *XTC4*, *XTC8* and *XTC9*
308 compared to at least one other clade.
309
310 **Discussion**
311
312 We have described a model for comparative functional genomics of *C. auris* in-host survival using
313 AK yolk-sac microinjections at a clinically relevant temperature in living tissue of a host featuring
314 mammalian-relevant innate immunity. All five clades demonstrated lethality, with a increase in virulence
315 during clades I and IV infections, consistent with clinical and laboratory findings (15). In-host growth was
316 similar across all clades and high enough to indicate a large enough *in vivo* fungal burden for robust bulk

317 transcriptome interrogation across the species. The contained nature of the yolk-sac provides a host
318 tissue growth medium that enables the assessment of pathogen survival and virulence strategies *in vivo*
319 and a straightforward experimental unit of host tissue without the challenges of pathogen RNA isolation
320 such as locating foci of infection in larger animals. Additional time-points could be an informative future
321 area of study to develop fine-resolution strain-specific transcription networks. Furthermore, the potential
322 of a translucent and genetically tractable fish embryo model could enable future visualisation of cellular
323 dynamics and genetic pathway manipulation (74). Thus, an AK yolk-sac microinjection model has the
324 potential to fill a substantial need for *in vivo* gene expression studies in general.
325
326 We investigated the host transcriptional response to *C. auris* infection, which featured an innate
327 immune response, as expected. The most highly up-regulated gene family included two haem oxygenase
328 (*HMOX*) genes. *HMOX* genes have been shown to mask iron from invading pathogens as a feature of
329 anti-*Candida* nutritional immunity (82), so presumably have a similar function against *C. auris*. This was
330 particularly notable given *HMOX* genes were up-regulated in response to clade IV infection, and the clade
331 IV isolate had a corresponding significant up-regulation of 3 haem transport-related *HTR* genes. In
332 addition to nutritional immunity genes, we found up-regulated heat shock and complement cascade
333 genes during infection, confirming the expected immune response to fungal infection (63, 64). Genes with
334 complex roles in immunity were up-regulated, such as *NLRP3*, for which *C. auris* may be less activating
335 than e.g. *C. albicans* (25, 83). It is notable that the yolk-sac model was not associated with histological or
336 transcriptional evidence of host neutrophil recruitment and activation, which may relate to the hypothesis
337 that *C. auris* is immunoevasive (31). Reference genome bias resulting from the available adult gill
338 transcriptome assembly (84) may limit detection of host gene expression features, so future long and
339 short read assembly from gene expression data across a range of larval stages could further
340 understanding of AK immunity.
341
342 We provided a thorough investigation of differential expression by *C. auris* during infection of host
343 tissue compared with *in vitro* conditions for the first time. The lack of a major distinction across time-points
344 (24 *vs* 48 HPI) indicates that the transcriptional activity of *C. auris* in-host was highly similar at these
345 stages. Six functional annotation terms (GO, KEGG pathway and PFAM domain) were significantly
346 enriched among genes that were up-regulated across all five clades, including sugar and siderophore
347 transporters. The enrichment of sugar transporters outside of nutrient-rich YPD-broth is unsurprising,
348 such as high-affinity glucose transporter *HGT12*, with evidence of redundancy in *C. albicans* (85–88), and
349 *HGT2*, part of an eight-gene “core filamentation response network” in *C. albicans* (89). More surprising
350 was the down-regulation of putative virulence factors such as Secreted Aspartyl Protease 3 (*SAP3*),
351 thought to be the most important SAP in *C. auris*, and required for virulence in a mouse model (23), and
352 Copper Superoxide Dismutase *SOD6*, which has been shown to be down-regulated in iron starvation

353 (90). Multi-drug efflux pumps such as *MDR2* (down-regulated *in vivo*) and *MDR1* (down-regulated *in vivo*
354 and in clades I and IV *vs* clades II and III) are understood to drive drug resistance through multiple but
355 unclear mechanisms in *C. auris* (91, 92); in-host down-regulation may indicate a fitness trade-off for
356 virulence *vs* drug resistance.
357
358 Mating type locus (*MTL*) genes have been hypothesised to contribute to virulence in fungal
359 species including *Cryptococcus neoformans* (93). Given that *C. auris* is assumed not to undergo meiotic
360 recombination (94), there is a question of what role *MTL*-associated genes play in pathogenesis and
361 morphology. Two of the three non-mating genes (*PAP1* and *PIKA*) in the *MTL* were up-regulated by more
362 virulent strains (I and IV) compared to the less virulent strains (II and III). Importantly, the two more
363 virulent clades (I and IV) contain *MTL**a*** rather than *MTL**α*** (clades II & III) (21), and clades V and VI
364 contain *MTL**a*** and *MTL**α*** respectively (11). Thus, it is unclear if the up-regulation of non-mating genes is a
365 *MTL* specific transcriptional nuance, or a feature of more highly virulent *C. auris* clades. The *MTL* also did
366 not feature prominently in the filamentation response observed in clade V, providing no evidence for an
367 obvious role for the *MTL* in such morphological changes.
368
369 Filamentation is an important pathogenicity trait in fungi, especially *Candida* species, although its
370 roles have been more poorly described in aquatic infections (95). We observed *in vivo* filamentation by a
371 representative strain of *C. auris* clade V, the basal/ancestral clade (96), accompanied by a genera-typical
372 filamentous gene expression signature. Specifically, we measured the up-regulation of *HGC1* and *UME6*,
373 which are two of the most important regulators of filamentation in *C. albicans*, and have recently been
374 described as drivers of *C. auris* filamentation and biofilm formation (97). The expression of adhesin *SCF1*
375 in filamenting clade V is noteworthy because its cationic adhesion mechanism has been postulated to be
376 consistent with adhesion mechanisms common to marine organisms including bivalves (19). The
377 generalist marine-isolated pathogen *C. haemulonii* has also displayed filamentation competence at lower
378 temperatures (98), consistent with an ancestral aquatic state.
379
380 Human histopathology reports of *C. auris* infection are rarely published and have not
381 demonstrated classical in-host filamentation, to our knowledge. An *ex vivo* human epithelial model using
382 a clade I isolate did demonstrate filamentous *C. auris* at 37 °C after injection into deeper dermis (99).
383 Clade III *C. auris* has also been observed to form filamentous/hyphal forms in *Galleria mellonella* injection
384 (58). Fan and colleagues have observed filamentous forms of *C. auris* across all four clades, even
385 demonstrating a higher virulence in the *G. mellonella* model (100), though the phenotype required
386 passage through a murine host with additional prolonged growth at 25 °C for at least 5 d before and after
387 injection (17). Other stimuli have induced filamentation in clade I isolates, such as hydroxyurea genotoxic
388 stress (101) and Hsp90 inhibition (102), where several up-regulated genes in *C. auris* filamentation

389 (*SCF1*, *IFF4* and *PGA31*) matched those in our study. Constitutive filamentous growth has also been
390 demonstrated with a transposon-mediated disruption of a long non-coding RNA (103), which sit adjacent
391 to chitin deacetylase *CDA2*, which was down-regulated at 24 HPI in our experiment during filamentation.
392 These findings indicate that hyphal formation is possible across *C. auris* clades.
393
394 A total of twelve siderophore transporters were up-regulated during infection, and four were
395 down-regulated, with three family members up-regulated in more virulent clades and five in the
396 filamentous clade V. The fact that siderophore transporter up-regulation has also been detected during
397 *ex vivo* whole blood infection by *C. auris* underscores the likelihood that our findings are clinically relevant
398 (28). Interestingly, this family of predicted xenosiderophore transporter genes is significantly expanded in
399 several members of the *Metschnikowiaceae* clade compared to other *Saccharomycetae* (21), raising
400 questions as to the roles of siderophore transporters in *C. auris* biology and evolution (104). Siderophore
401 synthesis may be unlikely in *C. auris*, given the lack of evidence in other *Candida* species (105). As a
402 result, *C. albicans* Sit1, which is required for virulence (106), is thought to be a xenosiderophore
403 transporter for iron-chelators produced by other microbes and specific to the ferrioxamine type common in
404 iron-poor ocean environments (107, 108). Siderophore transporters can also act intracellularly for
405 compartments such as the mitochondrion (109, 110), or act as efflux pumps for various molecules (111)
406 including trichothecene mycotoxins as identified by our functional annotations.
407
408 *C. auris* encodes a large expanded gene family of 17 siderophore transporters that we named
409 xenosiderophore transporter candidates (*XTC*) 1-12 and haem transport-related (*HTR*) genes 1-5, the
410 latter sharing sequence similarity with *S. pombe* low-affinity haem transporter Str3 (112). In other *Candida*
411 species such as *C. albicans*, iron assimilation is understood to be central for in-host survival (113, 114),
412 where deprivation triggers various pathogenic programmes such as alterations in cell surface beta-glucan
413 (115). Haem is acquired by *C. albicans* through vesicular endocytosis and CFEM-domain containing
414 proteins (116, 117) and does not contain *HTR* genes, suggesting a possible loss of transmembrane haem
415 transporters. The ubiquity of *HTR* across the fungal kingdom and lack of *XTC* genes in the three basal
416 fungal phyla suggest that *SIT1*/*HTC* could have arisen from a duplication of an *HTR*-related gene in the
417 *Dikarya* (the *Ascomycota* and *Basidiomycota*) with subsequent independent loss of both *XTC* and *HTC*
418 genes in multiple fungal lineages. Our identification of up-regulated *XTC* transport during infection
419 corroborates the findings of up-regulated *XTC2A-B* (*B9J08_1547-8*) in an *ex vivo* blood model of *C. auris*
420 infection (28). These findings together underline the importance of iron metabolism during infection, which
421 could be targeted in the clinic, e.g. *via* low-toxicity pyrvinium pamoate (118, 119).
422
423 We show for the first time an *in vivo* infection host tissue transcriptional profile for the critical
424 priority WHO human fungal pathogen *C. auris*. Representative strains from all five major clades of the

425 recent simultaneous emergences highlighted strain-specific differences in morphology, virulence and
426 gene expression. This study highlights the advantages and potential of a clinically relevant thermotolerant
427 yolk-sac injection model, adding to the debate around the putative marine origins of *C. auris*, and the
428 emergence of distinct clades. We demonstrate natural filamentation by clade V and virulence difference
429 for clades I and IV, and comprehensively describe associated gene expression. We indicate the
430 importance of the *XTC* and *HTR* gene clusters as recommended targets for investigation of fungal
431 biology, pathogenicity and treatment. These gene mechanisms likely enable *C. auris* to survive in host
432 tissue and provide a step forward in understanding the pathobiology of an emerging fungal pathogen and
433 global public health threat.
434
435 **Materials and methods**
436
437 Full details are given in SI Appendix. Briefly, wild-type adult AK were kept at the Aquatic Resources
438 Facility, Exeter, under Project Licence PP4402521. AK were kept in two 28 °C incubation tanks, with 12-
439 hour day and night light cycles and artificial enrichment foliage. Embryos were collected using three
440 plastic netted collection chambers per tank. Injection needles were prepared using borosilicate glass
441 capillaries (Harvard apparatus, USA) and a heated pulling system (heater level >62, PC-10, Narishige,
442 UK). We used tweezers to snap the tip to an estimated 1 mm graticule-measured aperture of 10-20 µm,
443 and sterilised needles before use with 253.7 nm UV light over 15 min (Environmental Validation
444 Solutions, UK). Injection bays were made with microwaved 1% agarose (Sigma, UK) in 1 g per 100 mL
445 ASW for up to 24 embryos in 100 mm petri dishes using custom-made molds in an inverted 60 mm petri
446 dish. Embryos were randomly chosen from each dish and the sequence of injection for each biological
447 repeat was randomly allocated by computer. *C. auris* yeasts were counted by haemocytometer and
448 added to 25 µL sterile filtered phenol red solution 0.5% (Sigma, UK) to a concentration of $0.5x10^8$ per mL
449 in 100 µL. Injection needles were loaded with 5 µL injection solution using 20 µL Microloader EpT.I.P.S.
450 (Eppendorf, UK) immediately before injection of up to 30 embryos before re-loading. Injections were
451 performed with 400-500 hPa injection pressure and 7-40 hPa compensation pressure over 100-200 ms
452 with the FemtoJet 4i (Eppendorf UK) using a micromanipulator (World Precision Instruments, UK) and a
453 Microtec HM-3 stereo dissection microscope (Optech, UK). To deliver a dose of approx. 500 yeasts in
454 10 nL solution, an injection bolus was administered to an estimated diameter of 0.2 – 0.3 mm (10-15% of
455 total embryo diameter) *via* a single chorion puncture. Any embryos that failed to meet these criteria for
456 injection were excluded. Control *in vitro* inoculations were microinjected as above into 1 mL YPD in
457 1.5 mL Eppendorf tubes before incubation without shaking at 37 °C for 24 h contemporaneously with
458 embryos as below.
459

460 We used an unblinded prospective virulence study comparing six groups of AK embryo yolk-sac
461 microinjection, including clades I-V of *C. auris*, and sham injections as the negative control. We used ≥23
462 embryos per condition based on a power calculation of σ = 0.25, significance = 0.05, power = 0.9, and δ
463 effect size of 25% mortality (two-sided t-test). After excluding embryos that were unhealthy or did not
464 complete successful microinjection, We included *n* = 10-13 embryos per group per experiment (total
465 *n* = 34-37 embryos per group). RNA was extracted from three embryos per condition per time-point (0, 24
466 and 48 HPI, *n* = 54) plus three embryos per time-point without any injection (*n* = 9, total *n* = 63) as a
467 control for the impact of microinjection.
468
469 We selected five *C. auris* strains to represent each major clade (**Table S1**). Culture stocks were
470 kept in -80 °C in Yeast extract Peptone Dextrose (YPD) broth (Sigma-Aldrich, UK) containing 25%
471 glycerol (ThermoFisher, UK) and plated onto YPD-agar (Sigma-Aldrich) for 48 h before inoculation and
472 overnight growth in 10 mL YPD broth at 30 °C in a shaking incubator at 200 RPM (Multitron, Infors HT,
473 UK). Five mL from each overnight culture was then centrifuged at 5000 g for 2 min before triple washing
474 in 1 mL autoclaved deionised water (DIW, Milli-Q, Merck, USA) to prevent aggregation (20), then re-
475 suspended again in 200 µL DIW.
476
477 Individual embryos were kept in 1 mL sterile filtered ASW per embryo in a 48 well flat bottom
478 plate (Corning, USA) sealed with Parafilm "M" (Bemis Company, USA) at 37 °C with passive
479 humidification using a 500 mL open glass beaker of water. Embryos were monitored for presence of heart
480 rate at 24-hourly intervals up to 7 d by stereo dissection microscope. Initial time of injection was
481 subtracted from each time-point to minimise bias between groups. Kaplan-Meier survival curves were
482 plotted with Log-Rank testing and Benjamini-Hochberg (BH) correction (120) using survival v.3.5.8 and
483 survminer v.0.4.9 packages in R v.4.4.0. Colony forming units (CFUs) were calculated by homogenisation
484 of embryos at 0, 24, and 48 HPI by autoclaved plastic micropestle in a 1.5 mL conical tube (Eppendorf,
485 UK) in 100 µL 10,000 U/mL penicillin/streptomycin (P/S) solution (Gibco, UK).
486
487 Dilutions were made with P/S solution and DIW in 1/10-10,000 and counts were adjusted
488 according to dilution after plating onto YPD agar plates and read after 72 h incubation at 30 °C. Statistical
489 testing between CFU numbers was performed with Wilcoxon testing and BH correction.
490
491 Total RNA was extracted using the Monarch® Total RNA Miniprep Kit (NEB, USA). Embryos
492 were flash frozen in liquid nitrogen, re-suspended in DNA/RNA Protection Reagent and disrupted with an
493 autoclaved plastic micropestle. Bead beating was performed in a FastPrep 24 homogeniser (MP
494 Biomedicals) with 0.5 mm zirconia/silica beads for 8 cycles of 35 s at 6 m/s plus 45 s on ice. Lysate was
495 recovered and incubated for 5 at 55 °C with proteinase K before addition of lysis buffer and RNA

496 purification following manufacturer's instructions. Library preparation and sequencing were performed by
497 the Exeter Sequencing Service. Samples were normalised and prepared using the NEBNext Ultra II
498 Directional RNA Library Prep - Poly(A) mRNA Magnetic Isolation Module following the standard protocol.
499 Libraries were sequenced on a Novaseq 6000 sequencer with 150bp paired-end reads. Reads were
500 trimmed with fastp (121) v.0.23.1 to remove reads <75 bases and trim based from the 3' end with q-score
501 <22. Quality control was performed with FastQC (https://github.com/s-andrews/FastQC) v.0.11.9 and
502 MultiQC (122) v.1.6.
503
504 We aligned sequences ($\bar{x}$ = 52.9 m reads per replicate, range 41.1-112.2 m) using the Trinity
505 pipeline (123) v.2.15.1 to the *C. auris* clade I B8441 reference genome (GCA_002759435.2) (21)
506 downloaded from GenBank (mean aligned reads in infected embryos 3.83 m, 0.81-13.1%). We further
507 aligned clade-specific reference genomes for each strain (**Table S1**), including clade II
508 (GCA_003013715.2) (4), III (GCA_002775015.1)(12), IV (GCA_008275145.1)(12) and V
509 (GCA_016809505.1)(96, 124, 125). We aligned conditions containing *A. dispar* to the *de novo* GJEY01
510 adult gill transcriptome assembly (84) downloaded from GenBank, for which we detected expression over
511 27,481 potential genes. Alignment was performed with Bowtie2 (126) v.2.5.1, transcript estimation with
512 RNA Seq by Expectation Maximisation (RSEM) (127) v.1.3.3, differential expression with EdgeR (128)
513 v.3.40.0, Samtools (129) v.1.17 and limma (130) v.3.54.0 using a false discovery rate (FDR) p-value cut-
514 off of 0.001 and a log fold change cut-off of +/-2.0. Principal components were calculated and plotted
515 using the prcomp function in Rv4.4.0 and ggfortify v.0.4.17 R package for fragments per kilobase per
516 million, and correlations plots from counts per million as per the default output of the Trinity pipeline. Log
517 fold change was plotted with ComplexHeatmap (131).
518
519 Gene ontology terms (132, 133) were assigned using DIAMOND (134) v.2.1.8 *via* the
520 DIAMOND2GO pipeline (135) for each of the *C. auris* reference genomes. KEGG terms (136) were
521 assigned using the BlastKOALA online platform using the eukaryote database (137). Protein FAMily
522 (PFAM) domains (138) were identified using the PFAM-A.hmm database
523 (https://ftp.ebi.ac.uk/pub/databases/Pfam/current_release/Pfam-A.full.gz) and HMMER and HMM Scan
524 (139) with a cut-off of $1e^{-5}$. Further domain-specific identification was performed with SignalP 5.0 (140),
525 DeepTMHMM 1.0 (141) and NetGPI 1.1 (142). To identify accessory genes across *C. auris* clades, we
526 used the Synima pipeline (143) with Orthofinder v2.5.5 (144) with additional reference genomes for
527 *C. albicans* (SC5314_GCA_000182965.3) and *C. haemulonii* (B11899_ASM1933202v1). Multiple
528 alignment of single copy orthologues as defined by Orthofinder was performed with Muscle v5.1 (145)
529 and a phylogeny was made with FastTree v2.1.11 (146). We visualised the structure using Alphafold v3
530 (147) and ChimeraX v1.8 (148). Clade I-V *C. auris* and *C. haemulonii SIT1* genes were aligned using
531 Muscle as above before using RAXML-NG v1.2.2 with 1000 bootstraps and the LG4X model (149), which

532 was visualised using ggtree v3.12.0.
533
534 **Data availability:** Raw reads have been deposited *via* NCBI/GEO *via* accession GSE277854. All
535 datasets and code required to make figures are available *via* Github
536 (https://github.com/hughgifford/Arabian_Killifish_C_auris_2024).
537
538 **Acknowledgements**
539
540 We acknowledge funding from the MRC Centre for Medical Mycology at the University of Exeter
541 (MR/N006364/2, MR/V033417/1), MRC Doctoral Training Grants MR/P501955/2 and MR/W502649/1,
542 Wellcome Trust (206412/A/17/Z), Wellcome Trust Career Development Award (215239/Z/19/Z) and
543 Wellcome Trust Fellowship (219551/Z/19/Z), National Centre for the Replacement, Refinement and
544 Reduction of Animals in Research (NC3Rs) (NC/X001121/1), and the NIHR Exeter Biomedical Research
545 Centre. TB also was supported *via* Elizabeth Ballou and a Sir Henry Dale Fellowship jointly funded by the
546 Wellcome Trust and the Royal Society (211241/Z/18/Z) and the Lister Institute. The views expressed are
547 those of the authors and not necessarily those of the NIHR or the Department of Health and Social Care.
548 We thank staff in the Aquatic Resource Center at the University of Exeter for husbandry of the fish and
549 the support for developing protocols for feeding, spawning, and raising new generations of this relatively
550 new model species, including Sam Worthington, Chloe Flint and Richard Silcox. We also thank the Exeter
551 Sequencing Service facility and support from Wellcome Trust Institutional Strategic Support Fund
552 (WT097835MF), Wellcome Trust Multi User Equipment Awards (WT101650MA and 218247/Z/19/Z),
553 Medical Research Council Clinical Infrastructure Funding (MR/M008924/1) and BBSRC LOLA award
554 (BB/K003240/1). We also thank the University of Exeter High-Performance Computing (HPC) facility
555 funded by the UK MRC Clinical Research Infrastructure Initiative (award number MR/M008924/1). We
556 thank Tanmoy Chakraborty, Dhara Malavia and Neil Gow for providing *C. auris* strains, Teigan Veale,
557 Sumita Roy, Jonathan Ball and Darren Thomson for assistance in microscopy and Chloe Pelletier for
558 advice on aggregation. We also thank Microtechnical Services, Exeter, UK, for assistance with
559 histological sectioning.
560
561 **References**
562
563 1. J. F. Meis, A. Chowdhary, *Candida auris*: A global fungal public health threat. *The Lancet*
564 *Infectious Diseases* **18**, 1298–1299 (2018).

565 2. WHO, World Health Organisation (WHO) fungal priority pathogens list to guide research,
566 development and public health action. (2022).
567 https://doi.org/https://www.who.int/publications/i/item/9789240060241.

568 3. W. G. Lee, *et al.*, First three reported cases of nosocomial fungemia caused by *Candida auris*.
569 *Journal of Clinical Microbiology* **49**, 4 (2011).

570 4. K. Satoh, *et al.*, *Candida auris* sp. Nov., a novel ascomycetous yeast isolated from the external
571 ear canal of an inpatient in a Japanese hospital. *Microbiology and Immunology* **53**, 41–44 (2009).

572 5. D. W. Eyre, *et al.*, A *Candida auris* outbreak and its control in an intensive care setting. *New*
573 *England Journal of Medicine* **379**, 1322–1331 (2018).

574 6. S. K. Taori, *et al.*, *Candida auris* outbreak: Mortality, interventions and cost of sustaining control.
575 *Journal of Infection* **79**, 601–611 (2019).

576 7. L. Shuping, *et al.*, High prevalence of *Candida auris* colonization during protracted neonatal unit
577 outbreak, South Africa. *Emerging Infectious Diseases* (2023). https://doi.org/10.3201/eid2909.230393.

578 8. R. D. Adam, *et al.*, Analysis of *Candida auris* fungemia at a single facility in Kenya. *International*
579 *Journal of Infectious Diseases* **85**, 182–187 (2019).

580 9. P. S. Prayag, S. Patwardhan, S. Panchakshari, P. A. Rajhans, A. Prayag, The dominance of
581 *Candida auris*: A single-center experience of 79 episodes of candidemia from western India. *Indian*
582 *Journal of Critical Care Medicine* **26**, 560–563 (2022).

583 10. T. Khan, *et al.*, Emergence of the novel sixth *Candida auris* clade VI in Bangladesh. *Microbiology*
584 *Spectrum* **12**, e03540–23 (2024).

585 11. C. Suphavilai, *et al.*, Detection and characterisation of a sixth *Candida auris* clade in Singapore: A
586 genomic and phenotypic study. *Lancet Microbe* **0** (2024).

587 12. S. R. Lockhart, *et al.*, Simultaneous emergence of multidrug-resistant *Candida auris* on 3
588 continents confirmed by whole-genome sequencing and epidemiological analyses. *Clinical Infectious*
589 *Diseases* **64**, 134–140 (2017).

590 13. H. Gifford, J. Rhodes, R. A. Farrer, The diverse genomes of *Candida auris*. *The Lancet Microbe* **0**
591 (2024).

592 14. S. A. Byun, *et al.*, Virulence traits and azole resistance in Korean *Candida auris* Isolates. *Journal*
593 *of Fungi* **9**, 979 (2023).

594 15. D. J. Santana, G. Zhao, T. R. O'Meara, The many faces of *Candida auris*: Phenotypic and strain
595 variation in an emerging pathogen. *PLOS Pathogens* **20**, e1012011 (2024).

596 16. J. Chen, *et al.*, Is the superbug fungus really so scary? A systematic review and meta-analysis of
597 global epidemiology and mortality of *Candida auris*. *BMC Infectious Diseases* **20**, 827 (2020).

598 17. H. Yue, *et al.*, Filamentation in *Candida auris*, an emerging fungal pathogen of humans: Passage
599 through the mammalian body induces a heritable phenotypic switch. *Emerging Microbes & Infections* **7**,
600 1–13 (2018).

601 18. C. Chadwick, M. D. Jesus, F. Ginty, J. S. Martinez, Pathobiology of *Candida auris* infection
602 analyzed by multiplexed imaging and single cell analysis. *PLOS ONE* **19**, e0293011 (2024).

603 19. D. J. Santana, *et al.*, A *Candida auris*-specific adhesin, Scf1, governs surface association,
604 colonization, and virulence. *Science* **381**, 1461–1467 (2023).

605 20. C. Pelletier, S. Shaw, S. Alsayegh, A. J. P. Brown, A. Lorenz, *Candida auris* undergoes adhesin-
606 dependent and -independent cellular aggregation. *PLOS Pathogens* **20**, e1012076 (2024).

607 21. J. F. Muñoz, *et al.*, Genomic insights into multidrug-resistance, mating and virulence in *Candida*
608 *auris* and related emerging species. *Nature Communications* **9**, 5346 (2018).

609 22. J. P. Richardson, *et al.*, Candidalysins are a new family of cytolytic fungal peptide toxins. *mBio*
610 **13**, e03510–21 (2022).

611 23. J.-S. Kim, K.-T. Lee, Y.-S. Bahn, Secreted aspartyl protease 3 regulated by the Ras/cAMP/PKA
612 pathway promotes the virulence of *Candida auris*. *Frontiers in Cellular and Infection Microbiology* **13**,
613 1257897 (2023).

614 24. M. V. Horton, *et al.*, *Candida auris* cell wall mannosylation contributes to neutrophil evasion
615 through pathways divergent from *Candida albicans* and *Candida glabrata*. *mSphere* **6**, e00406–21
616 (2021).

617 25. H. Weerasinghe, *et al.*, *Candida auris* uses metabolic strategies to escape and kill macrophages
618 while avoiding robust activation of the NLRP3 inflammasome response. *Cell Reports* **42**, 112522 (2023).

619 26. M. Lyman, Notes from the field: Transmission of pan-resistant and echinocandin-resistant
620 *Candida auris* in health care facilities - Texas and the District of Columbia, January-April 2021. *Morbidity*
621 *and Mortality Weekly Report* **70** (2021).

622 27. T. W. Wang, *et al.*, Functional redundancy in *Candida auris* cell surface adhesins crucial for cell-
623 cell interaction and aggregation. *Nature Communications* **15**, 9212 (2024).

624 28. S. Allert, *et al.*, From environmental adaptation to host survival: Attributes that mediate
625 pathogenicity of *Candida auris*. *Virulence* **13**, 191–214 (2022).

626 29. B. Fayed, *et al.*, Transcriptome analysis of human dermal cells infected with *Candida auris*
627 identified unique pathogenesis/defensive mechanisms particularly ferroptosis. *Mycopathologia* **189**, 65
628 (2024).

629 30. B. Yang, *et al.*, A correlative study of the genomic underpinning of virulence traits and drug
630 tolerance of *Candida auris*. *Infection and Immunity* **0**, e00103–24 (2024).

631 31. A. Balakumar, *et al.*, Single-cell transcriptomics unveils skin cell specific antifungal immune
632 responses and IL-1Ra- IL-1R immune evasion strategies of emerging fungal pathogen *Candida auris*.
633 *PLOS Pathogens* **20**, e1012699 (2024).

634 32. M. Bruno, *et al.*, Transcriptional and functional insights into the host immune response against the
635 emerging fungal pathogen *Candida auris*. *Nature Microbiology* **5**, 1516–1531 (2020).

636 33. Y. Wang, *et al.*, Innate immune responses against the fungal pathogen *Candida auris*. *Nature*
637 *Communications* **13**, 3553 (2022).

638 34. X. Wang, *et al.*, The first isolate of *Candida auris* in China: Clinical and biological aspects.
639 *Emerging Microbes & Infections* **7**, 1–9 (2018).

640 35. S. Fan, C. Li, J. Bing, G. Huang, H. Du, Discovery of the diploid form of the emerging fungal
641 pathogen *Candida auris*. *ACS Infectious Diseases* **6**, 2641–2646 (2020).

642 36. S. Fan, *et al.*, A biological and genomic comparison of a drug-resistant and a drug-susceptible
643 strain of *Candida auris* isolated from Beijing, China. *Virulence* **12**, 1388–1399 (2021).

644 37. S. Wurster, N. D. Albert, D. P. Kontoyiannis, *Candida auris* bloodstream infection induces
645 upregulation of the PD-1/PD-L1 immune checkpoint pathway in an immunocompetent mouse model.
646 *mSphere* **7**, e00817–21 (2022).

647 38. J. Bing, *et al.*, Rapid evolution of an adaptive multicellular morphology of *Candida auris* during
648 systemic infection. *Nature Communications* **15**, 2381 (2024).

649 39. R. Ben-Ami, *et al.*, Multidrug-resistant *Candida haemulonii* and *C. auris*, Tel Aviv, Israel.
650 *Emerging Infectious Diseases* **23** (2017).

651 40. C. L. Hager, E. L. Larkin, L. A. Long, M. A. Ghannoum, Evaluation of the efficacy of rezafungin, a
652 novel echinocandin, in the treatment of disseminated *Candida auris* infection using an
653 immunocompromised mouse model. *Journal of Antimicrobial Chemotherapy* **73**, 2085–2088 (2018).

654 41. M. Zhao, *et al.*, *In vivo* pharmacokinetics and pharmacodynamics of APX001 against *Candida*
655 spp. In a neutropenic disseminated candidiasis mouse model. *Antimicrobial Agents and Chemotherapy*
656 **62**, e02542–17 (2018).

657 42. S. Singh, *et al.*, The NDV-3A vaccine protects mice from multidrug resistant *Candida auris*
658 infection. *PLOS Pathogens* **15**, e1007460 (2019).

659 43. F. Zhang, *et al.*, A marine microbiome antifungal targets urgent-threat drug-resistant fungi.
660 *Science* **370**, 974–978 (2020).

661 44. J. E. Muñoz, *et al.*, Pathogenicity levels of Colombian strains of *Candida auris* and Brazilian
662 strains of *Candida haemulonii* species complex in both murine and *Galleria mellonella* experimental
663 models. *Journal of Fungi* **6**, 104 (2020).

664 45. M. Abe, *et al.*, Potency of gastrointestinal colonization and virulence of *Candida auris* in a murine
665 endogenous candidiasis. *PLoS One* **15**, e0243223 (2020).

666 46. L. Forgács, *et al.*, Comparison of in vivo pathogenicity of four *Candida auris* clades in a
667 neutropenic bloodstream infection murine model. *Emerging Microbes & Infections* **9**, 1160–1169 (2020).

668 47. F. Nagy, *et al.*, In vitro and in vivo interaction of caspofungin with isavuconazole against *Candida*
669 *auris* planktonic cells and biofilms. *Medical Mycology* **59**, 1015–1023 (2021).

670 48. L. Forgács, *et al.*, In vivo efficacy of amphotericin B against four *Candida auris* clades. *Journal of*
671 *Fungi (Basel, Switzerland)* **8**, 499 (2022).

672 49. S. Singh, *et al.*, Protective efficacy of anti-Hyr1p monoclonal antibody against systemic
673 candidiasis due to multi-drug-resistant *Candida auris*. *Journal of Fungi* **9**, 103 (2023).

674 50. E. A. Salama, *et al.*, Lansoprazole interferes with fungal respiration and acts synergistically with
675 amphotericin B against multidrug-resistant *Candida auris*. *Emerging Microbes & Infections* **13**, 2322649
676 (2024).

677 51. S. R. Torres, *et al.*, Impact of *Candida auris* infection in a neutropenic murine model.
678 *Antimicrobial Agents and Chemotherapy* **64**, e01625–19 (2020).

679 52. H. Xin, F. Mohiuddin, J. Tran, A. Adams, K. Eberle, Experimental mouse models of disseminated
680 *Candida auris* infection. *mSphere* **4**, e00339–19 (2019).

681 53. J. Rosario-Colon, K. Eberle, A. Adams, E. Courville, H. Xin, *Candida* cell-surface-specific
682 monoclonal antibodies protect mice against *Candida auris* invasive infection. *International Journal of*
683 *Molecular Sciences* **22**, 6162 (2021).

684 54. S. R. Torres, *et al.*, Assessment of environmental and occupational exposure while working with
685 multidrug resistant (MDR) fungus *Candida auris* in an animal facility. *Journal of Occupational and*
686 *Environmental Hygiene* **16**, 507–518 (2019).

687 55. A. M. Borman, Of mice and men and larvae: *Galleria mellonella* to model the early host-pathogen
688 interactions after fungal infection. *Virulence* **9**, 9–12 (2017).

689 56. D. Romera, *et al.*, The *Galleria mellonella* infection model as a system to investigate the virulence
690 of *Candida auris* strains. *Pathogens and Disease* **78**, ftaa067 (2020).

691 57. L. C. García-Carnero, *et al.*, Early virulence predictors during the *Candida* species–*Galleria*
692 *mellonella* interaction. *Journal of Fungi* **6**, 152 (2020).

58. V. Garcia-Bustos, *et al.*, Characterization of the differential pathogenicity of *Candida auris* in a *Galleria mellonella* infection model. *Microbiology Spectrum* **9**, e00013–21 (2021).

59. S. K. Carvajal, *et al.*, Pathogenicity assessment of Colombian strains of *Candida auris* in the *Galleria mellonella* invertebrate model. *Journal of Fungi* **7**, 401 (2021).

60. A. Hernando-Ortiz, *et al.*, Virulence of *Candida auris* from different clinical origins in *Caenorhabditis elegans* and *Galleria mellonella* host models. *Virulence* **12**, 1063–1075 (2021).

61. K. Spettel, *et al.*, *Candida auris* in Austria—what is new and what is different. *Journal of Fungi* **9**, 129 (2023).

62. S. Wurster, *et al.*, *Drosophila melanogaster* as a model to study virulence and azole treatment of the emerging pathogen *Candida auris*. *Journal of Antimicrobial Chemotherapy* **74**, 1904–1910 (2019).

63. V. Harpf, G. Rambach, R. Würzner, C. Lass-Flörl, C. Speth, *Candida* and complement: New aspects in an old battle. *Frontiers in Immunology* **11**, 1471 (2020).

64. J. Pechacek, M. S. Lionakis, Host defense mechanisms against *Candida auris*. *Expert Review of Anti-infective Therapy* **21**, 1087–1096 (2023).

65. L. Bavia, L. E. Santiesteban-Lores, M. C. Carneiro, M. M. Prodocimo, Advances in the complement system of a teleost fish, *Oreochromis niloticus*. *Fish & Shellfish Immunology* **123**, 61–74 (2022).

66. K. Buchmann, A. M. Karami, Y. Duan, The early ontogenetic development of immune cells and organs in teleosts. *Fish & Shellfish Immunology* **146**, 109371 (2024).

67. H. Tian, *et al.*, Cytokine networks provide sufficient evidence for the differentiation of CD4+ T cells in teleost fish. *Developmental & Comparative Immunology* **141**, 104627 (2023).

68. C. J. Johnson, J. M. Davis, A. Huttenlocher, J. F. Kernien, J. E. Nett, Emerging fungal pathogen *Candida auris* evades neutrophil attack. *mBio* **9**, e01403–18 (2018).

69. S. Pharkjaksu, N. Boonmee, C. Mitrpant, P. Ngamskulrungroj, Immunopathogenesis of emerging *Candida auris* and *Candida haemulonii* strains. *Journal of Fungi* **7**, 725 (2021).

70. R. S. Shapiro, L. E. Cowen, Uncovering cellular circuitry controlling temperature-dependent fungal morphogenesis. *Virulence* **3**, 400–404 (2012).

71. M. D. Leach, *et al.*, Hsf1 and Hsp90 orchestrate temperature-dependent global transcriptional remodelling and chromatin architecture in *Candida albicans*. *Nature Communications* **7**, 11704 (2016).

72. W. Xiao, *et al.*, Response and regulatory mechanisms of heat resistance in pathogenic fungi. *Applied Microbiology and Biotechnology* **106**, 5415–5431 (2022).

73. A. Akbarzadeh, E. H. Leder, Acclimation of killifish to thermal extremes of hot spring: Transcription of gonadal and liver heat shock genes. *Comparative Biochemistry and Physiology Part A: Molecular & Integrative Physiology* **191**, 89–97 (2016).

74. A. Hamied, *et al.*, Identification and characterization of highly fluorescent pigment cells in embryos of the Arabian killifish (*Aphanius Dispar*). *iScience* **23**, 101674 (2020).

75. A. Alsakran, *et al.*, Stage-by-stage exploration of normal embryonic development in the Arabian killifish, *Aphanius dispar*. *Developmental Dynamics* **n/a** (2024).

76. R. Minhas, *et al.*, The thermotolerant Arabian killifish, *Aphanius dispar*, as a novel infection model for human fungal pathogens. 2024.10.08.617174 (2024).

733 77. P. Arora, *et al.*, Environmental isolation of *Candida auris* from the coastal wetlands of Andaman
734 Islands, India. *mBio* **12**, e03181–20 (2021).

735 78. P. Escandón, Novel environmental niches for *Candida auris*: Isolation from a coastal habitat in
736 Colombia. *Journal of Fungi* **8**, 748 (2022).

737 79. V. Uden, M. C. Kolipinski, *Torulopsis haemulonii nov. spec.*, A yeast from the Atlantic Ocean.
738 *Antonie Van Leeuwenhoek* **28**, 78–80 (1962).

739 80. N. Burden, K. Chapman, F. Sewell, V. Robinson, Pioneering better science through the 3Rs: An
740 introduction to the national centre for the replacement, refinement, and reduction of animals in research
741 (NC3Rs). *Journal of the American Association for Laboratory Animal Science* **54**, 198–208 (2015).

742 81. M. S. Skrzypek, *et al.*, The *Candida* Genome Database (CGD): Incorporation of Assembly 22,
743 systematic identifiers and visualization of high throughput sequencing data. *Nucleic Acids Research* **45**,
744 D592–D596 (2017).

745 82. J. Potrykus, *et al.*, Fungal iron availability during deep seated candidiasis is defined by a complex
746 interplay involving systemic and local events. *PLOS pathogens* **9**, e1003676 (2013).

747 83. L. Kasper, *et al.*, The fungal peptide toxin candidalysin activates the NLRP3 inflammasome and
748 causes cytolysis in mononuclear phagocytes. *Nature Communications* **9**, 4260 (2018).

749 84. L. C. Bonzi, *et al.*, The time course of molecular acclimation to seawater in a euryhaline fish.
750 *Scientific Reports* **11**, 18127 (2021).

751 85. A. Varma, *et al.*, Molecular cloning and functional characterisation of a glucose transporter,
752 CaHGT1, of *Candida albicans*. *FEMS microbiology letters* **182**, 15–21 (2000).

753 86. L. Luo, X. Tong, P. C. Farley, The *Candida albicans* gene *HGT12* (Orf19.7094) encodes a
754 hexose transporter. *FEMS Immunology & Medical Microbiology* **51**, 14–17 (2007).

755 87. V. Brown, J. A. Sexton, M. Johnston, A glucose sensor in Candida albicans. *Eukaryotic Cell* **5**,
756 1726–1737 (2006).

757 88. D. E. Larcombe, *et al.*, Glucose-enhanced oxidative stress resistance-A protective anticipatory
758 response that enhances the fitness of *Candida albicans* during systemic infection. *PLOS Pathogens* **19**,
759 e1011505 (2023).

760 89. R. Martin, *et al.*, A core filamentation response network in *Candida albicans* is restricted to eight
761 genes. *PLOS ONE* **8**, e58613 (2013).

762 90. S. S. Schatzman, *et al.*, Copper-only superoxide dismutase enzymes and iron starvation stress in
763 *Candida* fungal pathogens. *The Journal of Biological Chemistry* **295**, 570–583 (2020).

764 91. J. M. Rybak, *et al.*, Abrogation of triazole resistance upon deletion of *CDR1* in a clinical isolate of
765 *Candida auris*. *Antimicrobial Agents and Chemotherapy* **63** (2019).

766 92. J. Li, A. T. Coste, D. Bachmann, D. Sanglard, F. Lamoth, Deciphering the Mrr1/Mdr1 pathway in
767 azole resistance of *Candida auris*. *Antimicrobial Agents and Chemotherapy* **66**, e00067–22 (2022).

768 93. S. Sun, M. A. Coelho, M. David-Palma, S. J. Priest, J. Heitman, The evolution of sexual
769 reproduction and the mating-type locus: Links to pathogenesis of *Cryptococcus* human pathogenic fungi.
770 *Annual Review of Genetics* **53**, 417–444 (2019).

771 94. Y. Wang, J. Xu, Population genomic analyses reveal evidence for limited recombination in the
772 superbug *Candida auris* in nature. *Computational and Structural Biotechnology Journal* **20**, 3030–3040
773 (2022).

95. D. P. Overy, T. Rämä, R. Oosterhuis, A. K. Walker, K.-L. Pang, The neglected marine fungi, *Sensu stricto*, and their isolation for natural products' discovery. *Marine Drugs* **17**, 42 (2019).

96. N. A. Chow, *et al.*, Potential fifth clade of *Candida auris,* Iran, 2018. *Emerging Infectious Diseases* **25**, 1780–1781 (2019).

97. M. Louvet, *et al.*, Ume6-dependent pathways of morphogenesis and biofilm formation in *Candida auris*. *Microbiology Spectrum* **0**, e01531–24 (2024).

98. Y. Deng, S. Li, J. Bing, W. Liao, L. Tao, Phenotypic switching and filamentation in *Candida haemulonii*, an emerging opportunistic pathogen of humans. *Microbiology Spectrum* **9**, e00779–21 (2021).

99. S. Seiser, *et al.*, Native human and mouse skin infection models to study *Candida auris*-host interactions. *Microbes and Infection* **26**, 105234 (2024).

100. S. Fan, *et al.*, Filamentous growth is a general feature of *Candida auris* clinical isolates. *Medical Mycology* **59**, 734–740 (2021).

101. G. Bravo Ruiz, Z. K. Ross, N. A. R. Gow, A. Lorenz, Pseudohyphal growth of the emerging pathogen *Candida auris* is triggered by genotoxic stress through the S phase checkpoint. *mSphere* **5**, e00151–20 (2020).

102. S. H. Kim, *et al.*, Genetic analysis of *Candida auris* implicates Hsp90 in morphogenesis and azole tolerance and Cdr1 in Azole Resistance. *mBio* **10**, e02529–18 (2019).

103. J. Gao, *et al.*, LncRNA DINOR is a virulence factor and global regulator of stress responses in *Candida auris*. *Nature Microbiology* **6**, 842–851 (2021).

104. A. D. Chybowska, D. S. Childers, R. A. Farrer, Nine things genomics can tell us about *Candida auris*. *Frontiers in Genetics* **11**, 351 (2020).

105. A. Ismail, G. W. Bedell, D. M. Lupan, Siderophore production by the pathogenic yeast, *Candida albicans*. *Biochemical and Biophysical Research Communications* **130**, 885–891 (1985).

106. P. Heymann, *et al.*, The Siderophore iron transporter of *Candida albicans* (Sit1p/Arn1p) mediates uptake of ferrichrome-type siderophores and Is required for epithelial invasion. *Infection and Immunity* **70**, 5246–5255 (2002).

107. R. M. Boiteau, *et al.*, Siderophore-based microbial adaptations to iron scarcity across the eastern Pacific Ocean. *Proceedings of the National Academy of Sciences* **113**, 14237–14242 (2016).

108. J. Park, *et al.*, Siderophore production and utilization by marine bacteria in the North Pacific Ocean. *Limnology and Oceanography* **68**, 1636–1653 (2023).

109. J. C. Renshaw, *et al.*, Fungal siderophores: Structures, functions and applications. *Mycological Research* **106**, 1123–1142 (2002).

110. T. C. Johnstone, E. M. Nolan, Beyond iron: Non-classical biological functions of bacterial siderophores. *Dalton Transactions* **44**, 6320–6339 (2015).

111. Y. Nakajima, *et al.*, Effect of disrupting the trichothecene efflux pump encoded by *FgTri12* in the nivalenol chemotype of *Fusarium graminearum*. *The Journal of General and Applied Microbiology* **61**, 93–96 (2015).

112. P. Xue, *et al.*, Heme sensing and trafficking in fungi. *Fungal Biology Reviews* **43**, 100286 (2023).

113. R. Fourie, O. O. Kuloyo, B. M. Mochochoko, J. Albertyn, C. H. Pohl, Iron at the Centre of *Candida albicans* Interactions. *Frontiers in Cellular and Infection Microbiology* **8**, 185 (2018).

815 114. A. Alselami, R. A. Drummond, How metals fuel fungal virulence, yet promote anti-fungal
816 immunity. *Disease Models & Mechanisms* **16**, dmm050393 (2023).

817 115. A. Pradhan, *et al.*, Non-canonical signalling mediates changes in fungal cell wall PAMPs that
818 drive immune evasion. *Nature Communications* **10**, 5315 (2019).

819 116. Z. Weissman, D. Kornitzer, A family of *Candida* cell surface haem-binding proteins involved in
820 haemin and haemoglobin-iron utilization. *Molecular Microbiology* **53**, 1209–1220 (2004).

821 117. C. Ding, *et al.*, Conserved and divergent roles of Bcr1 and CFEM proteins in *Candida parapsilosis*
822 *and Candida albicans*. *PLOS ONE* **6**, e28151 (2011).

823 118. C. Simm, *et al.*, Disruption of iron homeostasis and mitochondrial metabolism are promising
824 targets to inhibit *Candida auris*. *Microbiology Spectrum* **10**, e00100–22 (2022).

825 119. J. Zhang, *et al.*, Pyrvinium pamoate synergizes with azoles *in vitro* and *in vivo* to exert antifungal
826 efficacy against *Candida auris* and other *Candida* species. *Infection and Drug Resistance* **18**, 783–789
827 (2025).

828 120. Y. Benjamini, Y. Hochberg, Controlling the false discovery rate: A practical and powerful
829 approach to multiple testing. *Journal of the Royal Statistical Society Series B: Statistical Methodology* **57**,
830 289–300 (1995).

831 121. S. Chen, Y. Zhou, Y. Chen, J. Gu, Fastp: An ultra-fast all-in-one FASTQ preprocessor.
832 *Bioinformatics* **34**, i884–i890 (2018).

833 122. P. Ewels, M. Magnusson, S. Lundin, M. Käller, MultiQC: Summarize analysis results for multiple
834 tools and samples in a single report. *Bioinformatics* **32**, 3047–3048 (2016).

835 123. B. J. Haas, *et al.*, De novo transcript sequence reconstruction from RNA-seq using the Trinity
836 platform for reference generation and analysis. *Nature Protocols* **8**, 1494–1512 (2013).

837 124. M. Abastabar, *et al.*, *Candida auris* otomycosis in Iran and review of recent literature. *Mycoses*
838 **62**, 101–105 (2019).

839 125. J. F. Muñoz, *et al.*, Clade-specific chromosomal rearrangements and loss of subtelomeric
840 adhesins in *Candida auris*. *Genetics* **218**, iyab029 (2021).

841 126. B. Langmead, S. L. Salzberg, Fast gapped-read alignment with Bowtie 2. *Nature Methods* **9**,
842 357–359 (2012).

843 127. B. Li, C. N. Dewey, RSEM: Accurate transcript quantification from RNA-Seq data with or without a
844 reference genome. *BMC Bioinformatics* **12**, 323 (2011).

845 128. M. D. Robinson, D. J. McCarthy, G. K. Smyth, edgeR: A Bioconductor package for differential
846 expression analysis of digital gene expression data. *Bioinformatics* **26**, 139–140 (2010).

847 129. H. Li, *et al.*, The Sequence Alignment/Map format and SAMtools. *Bioinformatics* **25**, 2078–2079
848 (2009).

849 130. M. E. Ritchie, *et al.*, Limma powers differential expression analyses for RNA-sequencing and
850 microarray studies. *Nucleic Acids Research* **43**, e47 (2015).

851 131. Z. Gu, R. Eils, M. Schlesner, Complex heatmaps reveal patterns and correlations in
852 multidimensional genomic data. *Bioinformatics* **32**, 2847–2849 (2016).

853 132. M. Ashburner, *et al.*, Gene Ontology: Tool for the unification of biology. *Nature Genetics* **25**, 25–
854 29 (2000).

855 133. The Gene Ontology Consortium, *et al.*, The Gene Ontology knowledgebase in 2023. *Genetics*
856 **224**, iyad031 (2023).

857 134. B. Buchfink, K. Reuter, H.-G. Drost, Sensitive protein alignments at tree-of-life scale using
858 DIAMOND. *Nature Methods* **18**, 366–368 (2021).

859 135. C. Golden, D. J. Studholme, R. A. Farrer, DIAMOND2GO: A rapid Gene Ontology assignment
860 and enrichment tool for functional genomics. 2024.08.19.608700 (2024).

861 136. M. Kanehisa, M. Furumichi, Y. Sato, M. Kawashima, M. Ishiguro-Watanabe, KEGG for taxonomy-
862 based analysis of pathways and genomes. *Nucleic Acids Research* **51**, D587–D592 (2022).

863 137. M. Kanehisa, Y. Sato, K. Morishima, BlastKOALA and GhostKOALA: KEGG tools for functional
864 characterization of genome and metagenome sequences. *Journal of Molecular Biology* **428**, 726–731
865 (2016).

866 138. A. Bateman, *et al.*, The Pfam protein families database. *Nucleic Acids Research* **32**, D138–D141
867 (2004).

868 139. S. R. Eddy, Accelerated profile HMM searches. *PLOS Computational Biology* **7**, e1002195
869 (2011).

870 140. J. J. Almagro Armenteros, *et al.*, SignalP 5.0 improves signal peptide predictions using deep
871 neural networks. *Nature Biotechnology* **37**, 420–423 (2019).

872 141. J. Hallgren, *et al.*, DeepTMHMM predicts alpha and beta transmembrane proteins using deep
873 neural networks. (2022).

874 142. M. H. Gíslason, H. Nielsen, J. J. Almagro Armenteros, A. R. Johansen, Prediction of GPI-
875 anchored proteins with pointer neural networks. *Current Research in Biotechnology* **3**, 6–13 (2021).

876 143. R. A. Farrer, Synima: A synteny imaging tool for annotated genome assemblies. *BMC*
877 *Bioinformatics* **18**, 507 (2017).

878 144. D. M. Emms, S. Kelly, OrthoFinder: Phylogenetic orthology inference for comparative genomics.
879 *Genome Biology* **20**, 238 (2019).

880 145. R. C. Edgar, MUSCLE: Multiple sequence alignment with high accuracy and high throughput.
881 *Nucleic Acids Research* **32**, 1792–1797 (2004).

882 146. M. N. Price, P. S. Dehal, A. P. Arkin, FastTree 2 – approximately maximum-likelihood trees for
883 large alignments. *PLOS ONE* **5**, e9490 (2010).

884 147. J. Abramson, *et al.*, Accurate structure prediction of biomolecular interactions with AlphaFold 3.
885 *Nature* **630**, 493–500 (2024).

886 148. E. F. Pettersen, *et al.*, UCSF ChimeraX: Structure visualization for researchers, educators, and
887 developers. *Protein Science* **30**, 70–82 (2021).

888 149. A. Stamatakis, RAxML version 8: A tool for phylogenetic analysis and post-analysis of large
889 phylogenies. *Bioinformatics* **30**, 1312–1313 (2014).

890 **Figures and Tables**

891

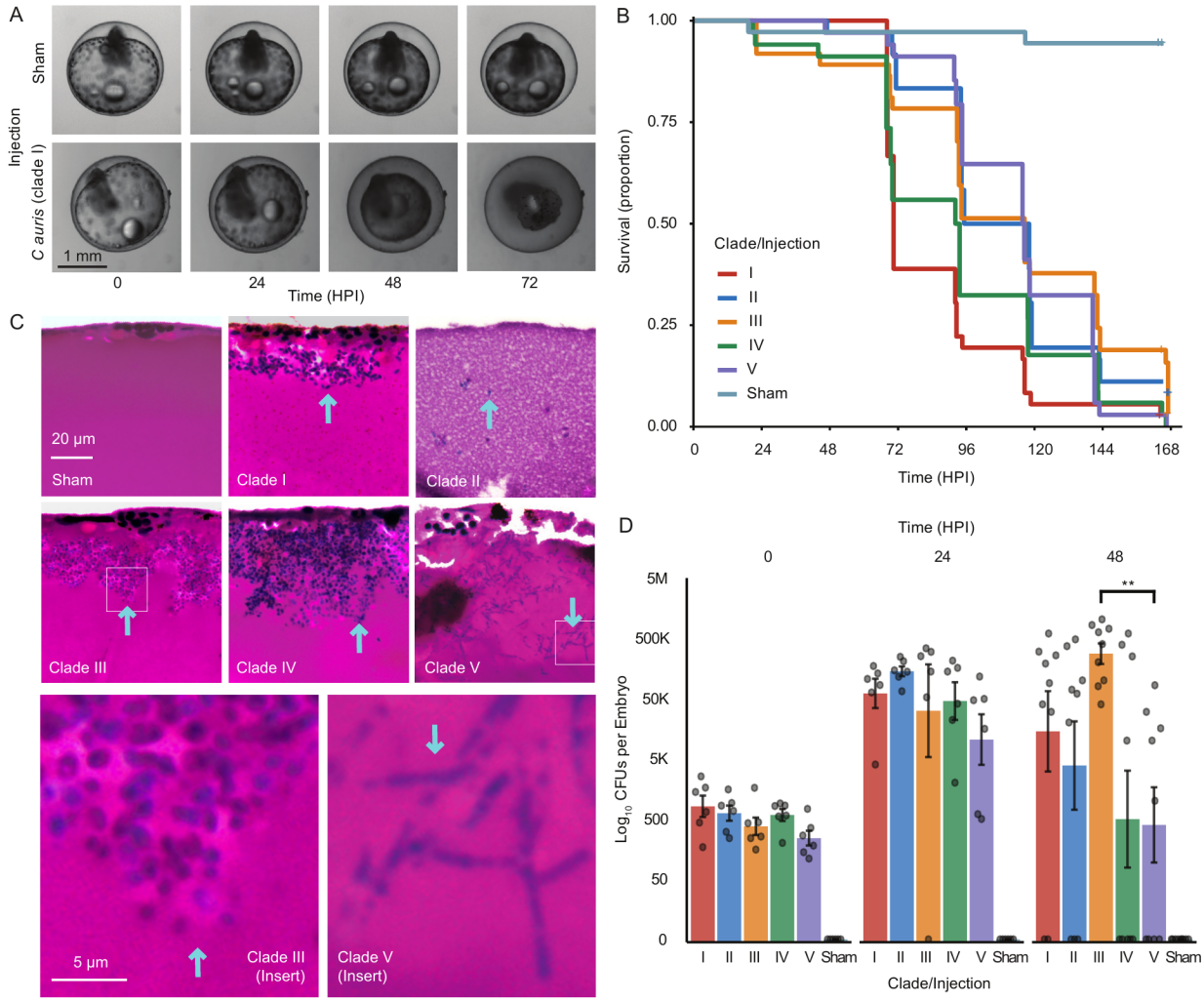

Figure 1: Modelling *C. auris* infection in the Arabian killifish **(A)** Illustrative time-lapse microscopy of embryo death including yolk-sac collapse during infection (clade I infection) or survival (sham injection) using Acquifer live imaging. **(B)** Survival curves for embryos injected with each *C. auris* clade or sham injection. Significance testing between groups is given in **Table S1**; hours post injection (HPI). **(C)** H&E Staining of AK yolk-sac at 48 HPI for each clade or sham injection; morphology is indicated by blue arrows, with insets indicating typical yeast (clade III) and filamentous morphology (clade V). The yolk-sac edge is oriented at the top. **(D)** Colony forming units (CFUs) per clade from embryos homogenised after injection as an indicator of injection dose and *in vivo* growth.

892

893

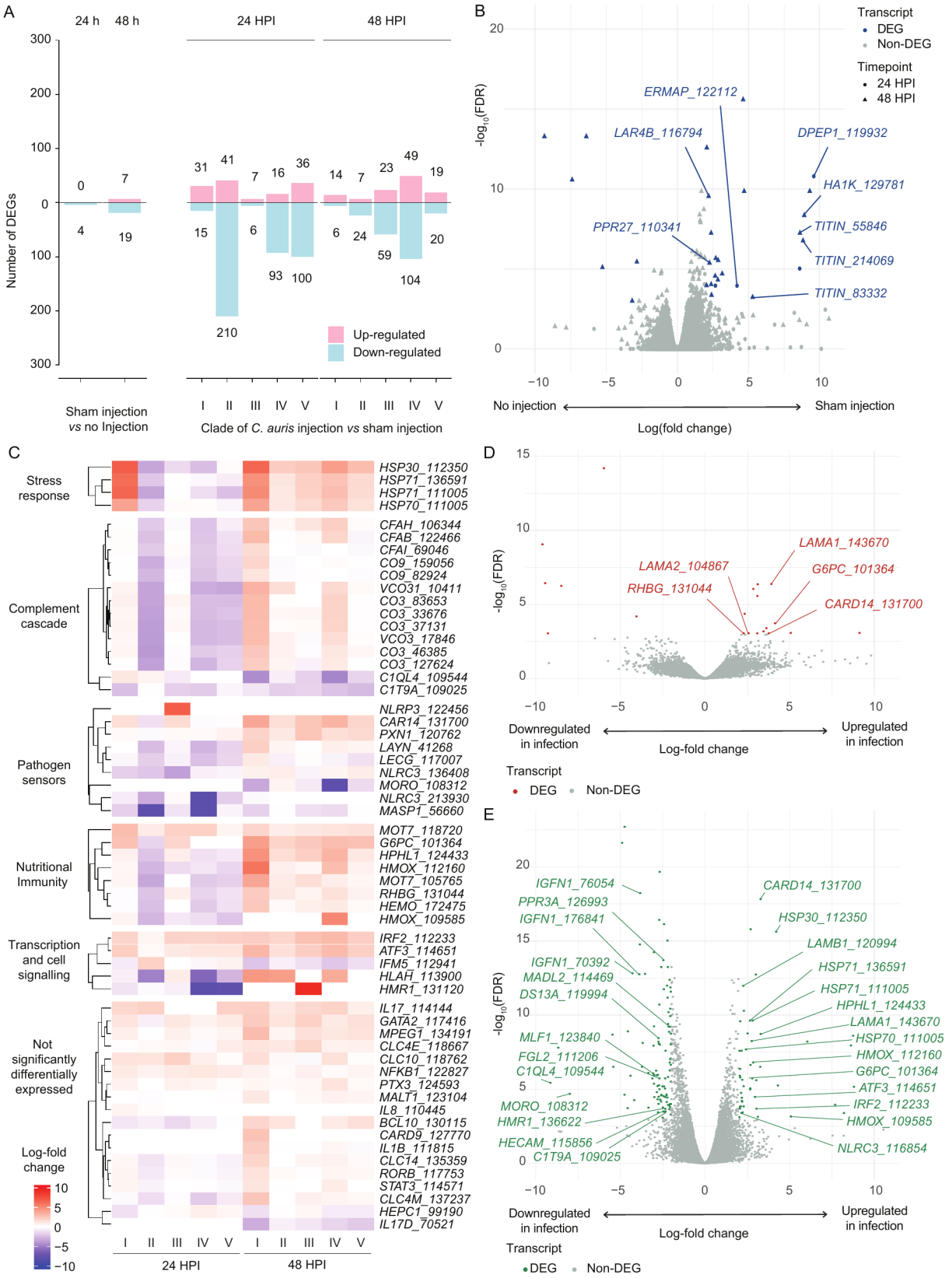
A
24 h
48 h
24 HPI
48 HPI
Number of DEGs
Up-regulated
Down-regulated
Sham injection vs no Injection
Clade of C. auris injection vs sham injection
B
Transcript
DEG
Non-DEG
Timepoint
24 HPI
48 HPI
-log10(FDR)
ERMAP_122112
LAR4B_116794
DPEP1_119932
HA1K_129781
PPR27_110341
TITIN_55846
TITIN_214069
TITIN_83332
No injection
Sham injection
Log(fold change)
C
Stress response
Complement cascade
Pathogen sensors
Nutritional Immunity
Transcription and cell signalling
Not significantly differentially expressed
Log-fold change
24 HPI
48 HPI
D
LAMA1_143670
LAMA2_104867
G6PC_101364
RHBG_131044
CARD14_131700
Downregulated in infection
Upregulated in infection
Log-fold change
Transcript
DEG
Non-DEG
E
IGFN1_76054
CARD14_131700
PPR3A_126993
HSP30_112350
IGFN1_176841
LAMB1_120994
IGFN1_70392
HSP71_136591
MADL2_114469
HSP71_111005
DS13A_119994
HPHL1_124433
LAMA1_143670
MLF1_123840
HSP70_111005
FGL2_111206
HMOX_112160
C1QL4_109544
G6PC_101364
ATF3_114651
MORO_108312
IRF2_112233
HMR1_136622
HMOX_109585
HECAM_115856
NLRC3_116854
C1T9A_109025
Downregulated in infection
Upregulated in infection
Log-fold change
Transcript
DEG
Non-DEG

894

895 **Figure 2:** AK host responses to *C. auris* infection: **(A)** Number of differentially expressed genes (DEGs)
896 for each of two comparisons, sham injection *vs* no injection (left panel), and *C. auris* injection *vs* sham
897 injection (right panel), at either 24 or 48 h post injection (HPI). **(B)** Volcano plot showing log-fold change
898 and significance according to $-\log^{10}$ false discovery rate (FDR) for sham injection *vs* no injection. **(C)**
899 Heatmap demonstrating log-fold change for differential expression between *C. auris* injection and sham
900 injection for groups of genes. **(D)** Volcano plot showing log-fold change and significance for DEGs
901 expressed during infection with clade I *C. auris* at 48 HPI. **(E)** Volcano plot showing log-fold change and
902 significance for DEGs expressed during infection with clade IV *C. auris* at 48 HPI.
903

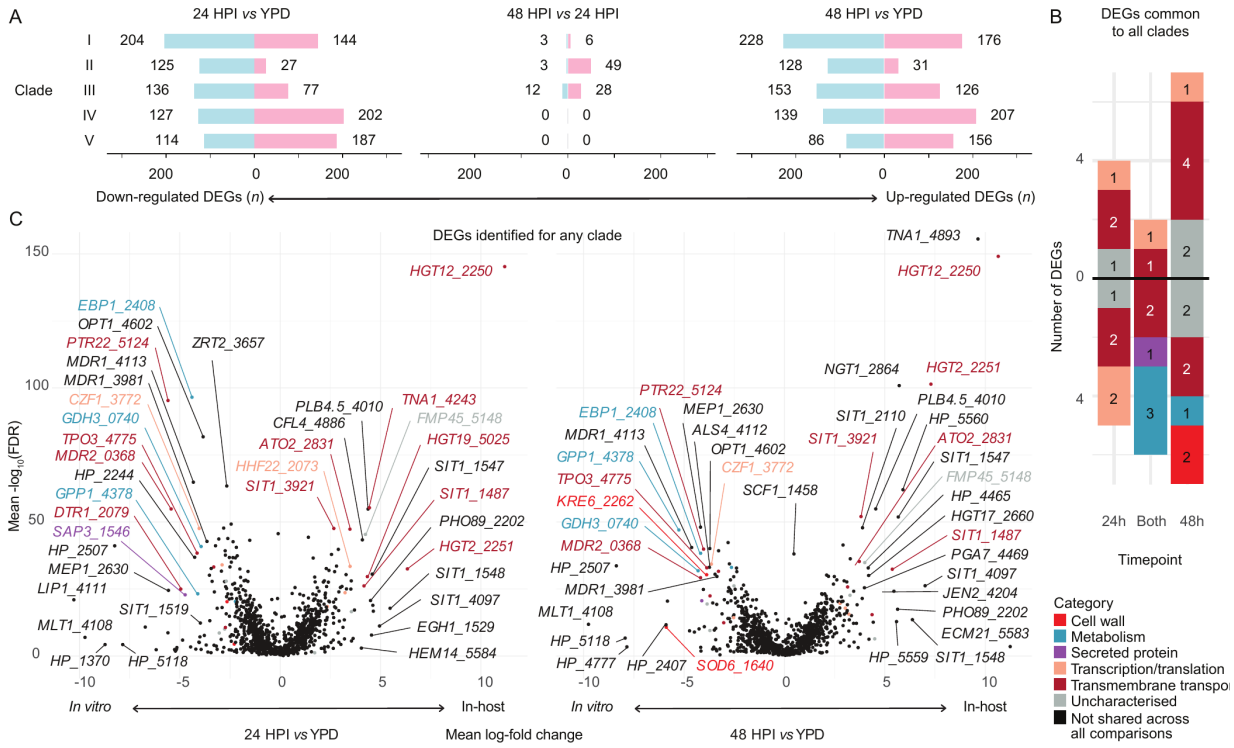

Figure 3: *C. auris* gene expression *in vivo vs in vitro* **(A)** Total DEGs per clade for each comparison between 24 h post injection (HPI), 48 HPI, and growth in YPD alone. **(B)** Combined set of significant DEGs common to all five clades between *in vivo* infection and *in vivo* growth in YPD. Genes are coloured by manually annotated category (**Table S3**). **(C)** Volcano plots demonstrate mean log-fold change for DEGs identified for any clade. Genes with infinite false discovery rate (FDR) are indicated with an arrow. Genes included in the combined set are coloured by category as per panel **B**.

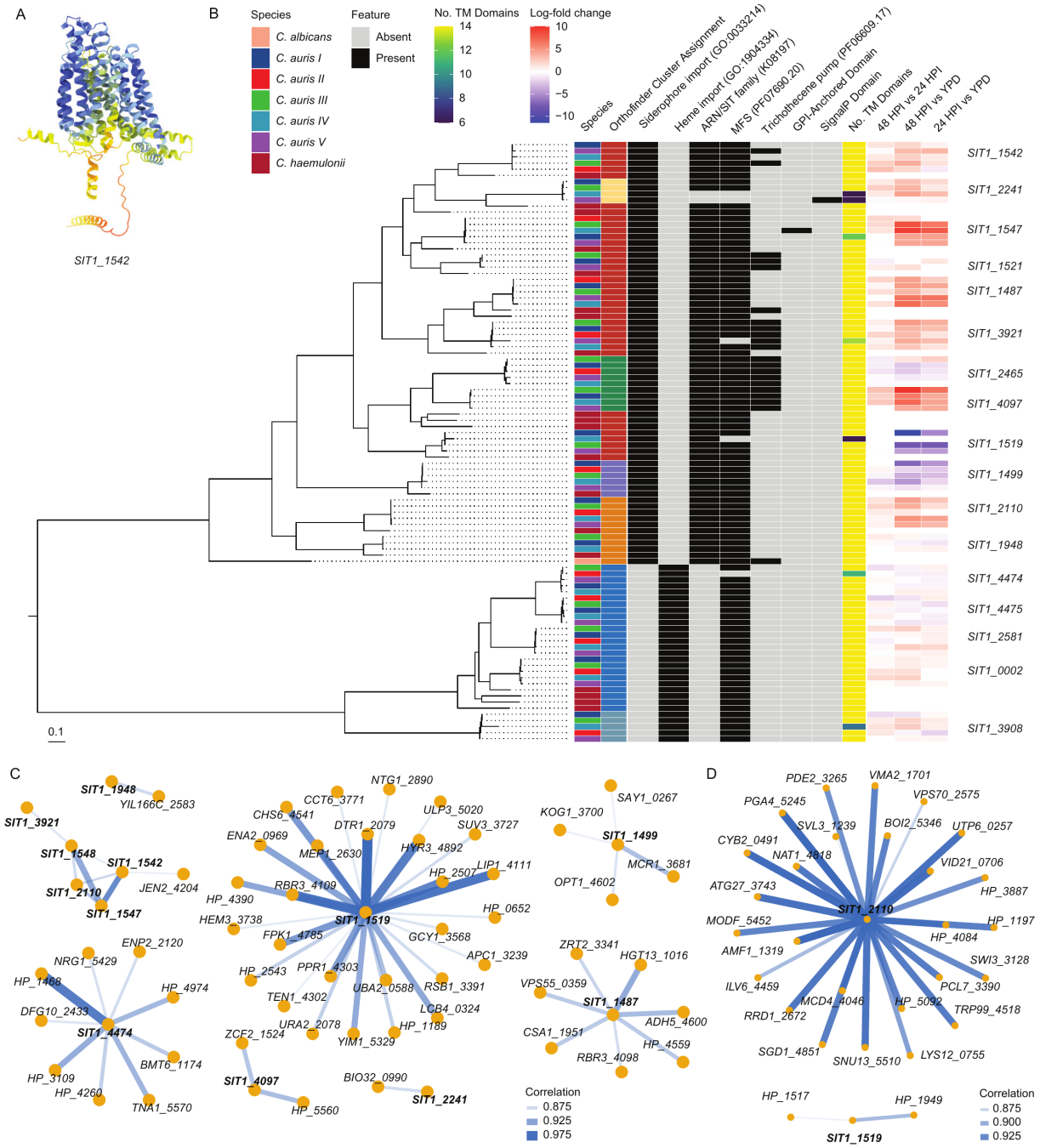

Figure 4: Xenosiderophore Transporter Analysis: **(A)** AlphaFold 3 predicted protein folding for peptide sequences for *SIT1* 1542, illustrating the conserved 14-transmembrane domain similarity across the families. **(B)** RAXML phylogeny using 1000 bootstraps and LG4X model of Muscle-aligned protein sequences for orthologues of *C. albicans* Siderophore Transport 1 *SIT1* gene. Scale bar indicates number of substitutions per site. Orthofinder cluster assignment notes which grouping each gene was

assigned to by our Synima/Orthofinder pipeline. **(C)** Pearson's correlation co-expression of associated gene expression involving siderophore transport candidate genes. **(D)** Pearson's correlation co-expression across available RNA-seq data from meta-analysis of 35 studies (**Table S4**), demonstrating a different set of transcriptional co-expression indicated by external experimental data.

906